NASA Technical Memorandum 4387

Flight Test Results of Riblets at Supersonic Speeds

Fanny A. Zuniga, Bianca T. Anderson,
and Arild Bertelrud

JUNE 1992

NASA

NASA Technical Memorandum 4387

Flight Test Results of Riblets at Supersonic Speeds

Fanny A. Zuniga and Bianca T. Anderson
Dryden Flight Research Facility
Edwards, California

Arild Bertelrud
High Technology Corporation
Hampton, Virginia

National Aeronautics and
Space Administration

Office of Management

Scientific and Technical
Information Program

1992

CONTENTS

TABLES

FIGURES

ABSTRACT

A flight experiment to test and evaluate the skin-friction drag characteristics of a riblet surface in turbulent flow at supersonic speeds was conducted at NASA Dryden Flight Research Facility. Riblets of groove sizes 0.0030 and 0.0013 in. were mounted on a F-104G flight test fixture. The test surfaces were surveyed with boundary-layer rakes and pressure orifices to examine the boundary-layer profiles and pressure distributions of the flow. Skin-friction reductions as a result of the riblet surface were reported based on measured differences of momentum thickness between the smooth and riblet surfaces obtained from the boundary-layer data. Flight test results for the 0.0030-in. riblets show skin-friction reductions of 4 to 8 percent for Mach 1.2 to 1.6 and Reynolds numbers ranging from 2 to 3.4 million per unit foot. The results for the 0.0013-in. riblets show skin-friction reductions of 4 to 15 percent for Mach 1.2 to 1.4 and Reynolds numbers ranging from 3.6 to 6 million per unit foot.

NOMENCLATURE

b	span length of the flight test fixture, 24 in.
C_d	drag coefficient for skin friction
C_F	average skin-friction coefficient
C_{Fr}	average skin-friction coefficient for riblet surface
C_{Fs}	average skin-friction coefficient for smooth surface
C_P	pressure coefficient, $(P - P_\infty)/q_\infty$
c	chord length of the flight test fixture, 81 in.
c_f	local skin-friction coefficient
FTF	flight test fixture
F_c	compressibility factor
H	shape parameter, where $H = \delta*/\theta$
HSCT	high-speed civil transport
h	peak-to-peak height in the riblet film, in.
$h+$	nondimensional riblet height, $h+ = h$ Re 1 ft $\sqrt{\frac{c_f}{2}}$
M_e	local Mach number at edge of boundary layer
M_∞	free-stream Mach number
P	local static pressure, lb/ft^2
P_∞	free-stream pressure, lb/ft^2
q_∞	free-stream dynamic pressure, lb/ft^2
Re	Reynolds number based on chord length of flight test fixture
Re/ft	Reynolds number per unit foot
Re_θ	Reynolds number based on momentum thickness

s spacing of peaks in riblet film, in.

U_e local velocity at edge of boundary layer, ft/sec

U_∞ free-stream velocity, ft/sec

u local velocity of boundary layer parallel to wall, ft/sec

$u+$ nondimensional wall parameter in scales of velocity

u_τ friction velocity, ft/sec

x horizontal distance from leading edge of flight test fixture, in.

y normal distance from test surface, in.

$y+$ nondimensional wall parameter in scales of length

z vertical distance from bottom edge of flight test fixture, in.

α angle of attack, deg.

δ boundary-layer thickness, in.

$\delta*$ displacement thickness, in.

θ momentum thickness, where $\theta = \int_0^\delta \frac{\rho u}{\rho e U e}(1 - \frac{u}{Ue})dy$

$\theta_{aft,r}$ momentum thickness at aft end of test section for riblet surface

$\theta_{aft,s}$ momentum thickness at aft end of test section for smooth surface

θ_{fwd} momentum thickness at forward station of test section

μ viscosity coefficient, lb/ft·sec

ρ density of fluid at local conditions, slug/ft^3

ρ_∞ density of fluid at free-stream conditions, slug/ft^3

ν_w kinematic viscosity at the wall, ft^2/sec

τ_w shear stress at the wall, lb/ft^2

INTRODUCTION

Currently, NASA is developing new technologies for the design and development of a high-speed civil transport (HSCT). A primary concern in the design of an HSCT is how to improve the aerodynamic efficiency or overall lift-to-drag ratio. Typically, turbulent skin-friction drag accounts for approximately 40 percent of the total drag for an HSCT configuration. Therefore, reduction of this drag may not only improve aerodynamic efficiency, but can also lead to appreciable fuel savings.

One successful method to reduce turbulent skin-friction drag at subsonic speeds has been to reconfigure smooth aerodynamic surfaces with narrow grooves in the direction of the stream. These microscopic longitudinal grooves embedded in the surface have been commonly referred to as riblets. Briefly, the grooves in a riblet surface act to reduce turbulent skin-friction drag by diminishing the momentum losses of the low-speed region of fluid near the wall (ref. 1). Over the past several years, many

investigations have been conducted to determine how these grooves interact within the turbulent boundary layer (ref. 2) and to evaluate the drag reduction performance of this riblet concept. References 3 through 6 report skin-friction reductions of 6 to 8 percent for subsonic flow.

To extend these results into the supersonic flow regime, two wind-tunnel tests have recently been conducted. Gaudet's results (ref. 7) showed drag reduction of 7 percent at Mach 1.2. Robinson's results, reference 8, concluded that changes in turbulence intensity caused by the application of riblets in a supersonic boundary layer were in agreement with riblet results obtained at low speeds. Although drag-reduction performance was not measured in Robinson's experiment, his findings suggested that riblets could be effective for reducing friction drag at supersonic as well as subsonic speeds. To date, these are the only two sets of supersonic wind-tunnel data obtained. Therefore, to verify the performance of riblets at supersonic speeds, flight data over a supersonic Mach number range were needed.

The objectives of the present flight experiment were (1) to determine if the application of riblet material to a surface in turbulent flow can reduce skin-friction drag at supersonic speeds, and (2) to verify that the physical characteristics of the riblets that yield maximum skin-friction reduction (ref. 2) are consistent with previous subsonic investigations. To meet these objectives, two riblet sizes were tested. Each was tested in a design Reynolds number range selected to yield maximum skin-friction reduction.

The F-104G flight test fixture (FTF) (ref. 9) was the test facility for this experiment. Each side of the fixture provided a test area of 56.75 in. by 19 in. The right side was the test side; comparisons of the average skin-friction results with and without riblets were made. The left side was used strictly as the control side to monitor the flow and ensure repeatable flow condition of the test points.

Two identical boundary-layer rakes were used to survey the boundary layer of the flow with the same differential pressure transducer over the control and test surfaces. The differences in measured momentum thickness between the smooth and riblet test surfaces on the right side of the FTF were calculated from the boundary-layer profiles generated by the respective surfaces. These differences led to measurements of average skin-friction reduction as a result of the application of riblets. The results of this investigation, with a complete description of the experiment setup and data analysis, will be presented here.

FLOW PHYSICS OF RIBLETS

The concept of skin-friction reduction through modification of the wall structure is not new. Over the past three decades, several approaches, as described in reference 1, have evolved into the present drag-reduction technique known as riblets. One of the earliest investigations of more than 30 years ago, reference 10, examined shark skin and its interaction with the flow structure.

Until approximately a decade ago, it was commonly assumed that turbulent structures were adequately described through statistical quantities. Time averages of turbulence in terms of velocity, pressure, and temperature fluctuations, as well as cross-correlations of these, were examined and used to develop turbulence models. In some cases, however, a time-dependent description was necessary to show an identifiable sequence of events. These events are commonly called coherent structures. The

motion is strongly three dimensional, and may be described simply as bursts of flow moving away from the surface followed by sweeps moving toward the surface. More recently, discussions of coherent structures have led to many studies in which various schemes to manipulate the coherent structures, in particular riblets, have been attempted.

Walsh (ref. 2) conducted several investigations in determining how the physical geometry of the riblets (i.e., the size and shape of the grooves) affect the performance of riblets. Aspect ratio, or the height (h) and spacing (s) of the grooves, as well as the shape of the grooves, such as corner rounding, were taken into consideration. As a result, it was demonstrated that an aspect ratio of 1 (that is, $h = s$) was optimum for maximum drag reduction performance (fig. 1). For best performance, grooves of triangular shape were also concluded to be optimum.

In addition, Walsh found that optimum skin-friction drag reduction in subsonic flow occurs at a nondimensional riblet height, $h+$, of 12 to 15 wall units (ref. 2). By interpreting $h+$ values to Reynolds numbers, a design range of Reynolds numbers was determined for the present flight experiment based on Walsh's subsonic data to yield optimum skin-friction drag reduction.

Choi (ref. 11) conducted detailed investigations examining the effects of riblets on the structure of the turbulent boundary layer. The results from Choi's subsonic investigations yielded two important conclusions. First, riblets act in thickening the sublayer. The law of the wall for the time-averaged boundary-layer profile was commonly taken to be $u+ = 5.45 \log(y+) + 5.45$. In the presence of a riblet surface, the law of the wall was altered to $u+ = 5.5 \log(y+) + 6.89$. In Robinson's experiment, the effect of the riblet surface of nondimensional height $h+ = 15$ also resulted in thickening the sublayer, corresponding to an outward shift of 6.8 in $y+$ wall units.

Second, Choi's investigation concluded that riblets cause an appreciable reduction of turbulence intensity level in the inner regions of the boundary layer. His riblet data showed a reduction in level from $y+ = 18$ out to $y+ = 70$, where the smooth wall turbulence production was at its maximum at $y+ = 50$. Robinson performed a similar documentation of the turbulence intensity for a supersonic boundary layer at Mach 2.97. His findings showed similar results. Although a reduction of turbulence intensity level usually indicates a reduction in turbulence production in the boundary layer, it does not necessarily translate to a reduction in skin-friction drag.

These results as well as the results of previous investigations (ref. 1–8 and 11) also imply that the effects of riblets are locally confined to the riblet surface and are kept within the wall structure of the turbulent boundary layer. In only one boundary-layer thickness downstream of the riblet surface, the mean velocity profile can be expected to return to its normal characteristics. Therefore, the traditional relationships available for the integral properties of turbulent boundary layers were used in the data analysis.

EXPERIMENT DESCRIPTION AND TEST CONDITIONS

A specially equipped F-104G aircraft served as the carrier vehicle for the supersonic riblet experiment. The aircraft instrumentation included an uplink trajectory guidance system (ref. 12). This uplink system indicated differences between desired and actual flight conditions, specifically Mach number,

altitude, and angle of sideslip. The pilot flew all test points at steady level flight conditions using this uplink system to ensure accuracy and repeatability of the data.

The FTF, a fin-like shape with low aspect ratio, was mounted vertically on the lower centerline of the F-104G carrier aircraft, as shown in figure 2. The chord length of the FTF is 81 in., the semispan is 24 in., and for the major part of its length, except the forebody, the thickness is a constant 6.4 in. As described in reference 9, the FTF was specially developed as a unique research facility for conducting aerodynamic and fluid-mechanic experiments in flight.

The FTF was equipped with interchangeable noseshapes (fig. 3). This experiment used an elliptical cross section made of foam and fiberglass. This noseshape allowed panels containing the riblet material to be attached to the sides of the FTF, and provided a smooth continuous surface from the leading edge of the FTF to the test surface.

A transition grit strip ensured a known and repeatable transition location on the FTF. This transition strip was positioned 9.38 in. from the trailing edge of the noseshape, and placed on both sides of the FTF. The transition strip was 0.125-in. wide and made of No. 46 carborundum grains. The selection of the grit size was determined using reference 13.

This experiment used measurements on both sides of the FTF; see figure 3. Each test surface covered an area of 56.75-in. long by 19-in. wide. The left side was used strictly as a control side to monitor the flow and ensure repeatable flow condition of test points. After some baseline flights with smooth panels on both sides, riblet material was applied to the right side test surface only, 15-in. aft of the leading edge. Adhesive-backed plastic film, embedded with longitudinal, microscopic grooves in its surface served as the riblet material in this experiment. A schematic of this grooved, plastic film or riblet film is shown in figure 1.

The size and shape of the grooves of the riblet film tested in this experiment were selected to yield optimum skin-friction reduction based on the data presented by Walsh (ref. 2). Two sizes of riblet film were evaluated: one having a height and spacing of 0.0013 in. and one a height and spacing of 0.0030 in. The grooves in the riblet film were symmetrical and triangular shaped with relatively sharp peaks and valleys.

Figure 4 shows the flight test conditions obtained for this experiment along with the flight envelope of the F-104/FTF. For the 0.0030-in. riblets, Reynolds numbers ranged from 2 to 3.4 million Re/ft and Mach numbers ranged from 1.2 to 1.6. For the 0.0013-in. riblets, Reynolds numbers ranged from 3.6 to 6 million Re/ft and Mach numbers from 1.2 to 1.4. Shown also in this figure are riblet design test conditions as determined by reference 2. As discussed earlier, these design test conditions were selected to provide optimum skin-friction reduction results based on subsonic data (ref. 2). As can be seen, both design and off-design test conditions were obtained for 0.0013- and 0.0030-in. riblet film.

INSTRUMENTATION

The instrumentation for the control and riblet test surfaces consisted of two boundary-layer rakes, two rows of flush static pressure orifices, and two rows of six modified Preston tubes positioned spanwise

at the trailing edges of the FTF. Figures 3(a) and (b) show right- and left-side views of the experiment setup. All research and airdata parameters were digitally encoded using pulse code modulation, and were recorded onboard and telemetered to ground-based recorders.

Boundary-layer rakes were used to determine the boundary-layer profiles and average skin-friction coefficients at the end of each test section (fig. 3). Each boundary-layer rake consisted of 20 total pressure probes positioned 71.75-in. aft of the leading edge, $x/c = 0.886$. Figure 5 illustrates the boundary-layer rake mounted on the FTF. These rake probes were mounted along a 5-in. plate at the end of the riblet and control test sections, canted 30° from the plane of the FTF surface. Canting the rake plate allowed more probes to be located in the boundary layer with minimum probe interference. With this type of orientation, the last probe on the rake was 2.5 in. from the surface. Each rake was oriented streamwise to the flow. Table 1 lists the distance of each probe from the surface.

A mechanical scanning pressure module or scani-valve, connected to the probes by tubing approximately 2-ft. long, measured the pressure at each probe. Pressures from both rakes were measured alternately from left to right. These pressures were compared with a reference pressure measured with a 17-bit digital absolute pressure transducer. Probes from both rakes were measured by the same $\pm$ 12.5-lb/in^2 differential pressure transducer. Using one pressure transducer minimized the error in determining the boundary-layer pressure distribution.

The sampling rate for each pressure probe was 0.41 samples/sec. Data were averaged over 20 sec for each test condition. Pressures from the differential pressure transducer were estimated to be accurate to within $\pm$ 0.06 lb/in^2.

Two rows of 14 flush static pressure orifices each was positioned along the top and bottom of the left side of the FTF, as shown in figure 3(b). The surface static pressures were used to examine the FTF chordwise pressure distribution at flight conditions. The bottom row was 3.75 in. above the bottom edge of the panel, and the top row was 16.81 in. above the bottom edge of the panel. Table 2 presents the chordwise orifice locations for the top and bottom rows on the left side of the FTF.

Each flush static orifice had an inside diameter of 0.030 in. Pressures were measured with $\pm$ 5- and $\pm$ 10-lb/in^2 electronic scanning pressure modules. Plastic tubing ran from each orifice to a pressure transducer. The maximum length of tubing between the orifices and the pressure transducers was approximately 3 ft.

A row of six modified Preston tubes was positioned spanwise aft of the test section for each side of the FTF, 75.75 in. from the leading edge. Although the Preston tubes measured static and total pressures at each station (ref. 14), only the static pressure measurements were used to determine the spanwise pressure distributions at the boundary-layer-rake chord location. Figure 5 illustrates some of these Preston tubes positioned alongside the boundary-layer rake. Table 3 shows the location of each Preston tube on the FTF.

Pressure data from the static pressure orifices and modified Preston tubes were recorded at 7.8 samples/sec. The pressures from these transducers were accurate to within $\pm$ 0.03 lb/in^2. The coefficients of pressure were accurate to within 0.01 for the flight conditions tested.

The F-104G aircraft was instrumented with a standard NACA noseboom (ref. 15) to measure total and static pressure, angle of attack, and angle of sideslip. The FTF was also instrumented with a noseboom that provided the FTF with an independent measurement of Mach number, dynamic pressure, and altitude. The FTF noseboom airdata were uplinked to the pilot in flight for trajectory guidance use; this airdata were also used in the data analysis.

DATA ANALYSIS

The resultant change in skin-friction drag caused by the application of riblets was determined by measuring and comparing the boundary-layer mean velocity profiles for the smooth and riblet surfaces. In addition to measuring the mean velocity profile aft of the riblet surface, it was also necessary to include the initial conditions forward of the riblet surface. A practical solution to estimating the initial conditions was to use the measured pressure distributions along the top and bottom rows of the FTF along with the measured momentum thickness, and then to allow a boundary-layer code to compute the initial conditions.

For this computational analysis, a three-dimensional finite-difference code by Bradshaw et al. (ref. 16) was used to compute the flow along the smooth right side of the FTF using the measured aft boundary-layer characteristics including momentum thickness, shape factor, and local pressure coefficient. By varying the initial conditions, computations were iterated until the appropriate measured momentum thickness was matched at the rake location for the smooth surface. In this way, the forward momentum thickness, θ_{fwd}, was determined.

The aft momentum thickness values from flight, θ_{aft}, were calculated by integrating the boundary-layer velocity profile (ref. 17) from the measured boundary-layer-rake data. Differences between the forward- and aft-momentum thickness values for the smooth and riblet test surfaces were then calculated.

To determine the change in skin-friction drag caused by the application of riblets, the momentum integral equation was used (ref. 17). Initially, a simplified approach was used which assumed the flow over the test section to be two dimensional or that of zero pressure gradient and zero crossflow. This assumption led to the following simplified linear relationship:

$$C_F = 2\frac{\theta_{\text{aft}} - \theta_{\text{fwd}}}{\Delta x}$$

Skin-friction changes between riblet and smooth surfaces were then computed using the following:

$$\frac{C_{F_r}}{C_{F_s}} = \frac{\theta_{\text{aft,r}} - \theta_{\text{fwd}}}{\theta_{\text{aft,s}} - \theta_{\text{fwd}}}$$

Since the riblet experiment included regions of fairly strong pressure gradient caused by shock interaction from the F-104G aircraft, a more extensive analysis of the data was used to verify the assumptions of the simplified approach. This analysis used the full momentum equation including the pressure coefficients and the shape parameter. The simplified approach to the data analysis was

concluded to be sufficient, and therefore, only those results are presented. However, the detailed data analysis is described in the following.

The analysis was performed for the forward and aft locations using a compressible version of the Squire-Young method (ref. 18) by Lock (ref. 19). An interpretation of the data including all terms eventually contributing to the far downstream wake behind the FTF was also included, since this would reveal the proper drag effects corresponding to any changes in local flow over the FTF.

The measured boundary-layer data at one location were related to its far downstream value through Lock's equation:

$$\frac{\theta_\infty}{\theta_T} = \frac{\rho_T}{\rho_\infty}\left(\frac{U_{eT}}{U_\infty}\right)^{\left(\frac{1}{2}H_T + H_\infty + 4\right)}$$

Here θ_T, ρ_T, U_{eT}, and H_T are local values. The subscript T denotes trailing-edge values, but the properties may be determined at any location along the FTF. One way of looking at the implications of this equation is to evaluate the properties at any location along the airfoil. It will then be a measure of the integrated boundary-layer development from the leading edge back to the particular location. Any wall shear occurring farther back will increase the value of the momentum thickness in the far wake. The far-wake value of the momentum thickness is related to the momentum thickness by the simple expression $C_d = 2\theta_\infty$. A change in momentum thickness at any particular location will be magnified or attenuated depending primarily on C_p distribution (U_e or M_e development), but also depending on the shape parameter, H.

A change in pressure distribution along the FTF will be reflected by a considerable change in momentum thickness, θ. A decrease in θ locally is possible and common. In the present experiment, changes in pressure distribution must be accounted for when evaluating the experimental velocity profiles, since they may completely mask the effects of the riblet surface.

Figure 6(a) illustrates how the use of θ may cause a misinterpretation of effects depending on the location. If θ had been measured farther forward of the rake location, $x/c = 0.886$, the relation between results would have been misinterpreted. In this case, an interpretation of C_d, figure 6(b), was needed for proper verification of results. In the present report, estimates θ and C_d were interpreted for verification of results. In most cases there was good agreement, and therefore, only results from the simplified approach are presented in this report.

RESULTS AND DISCUSSION

The flow environment of the F-104G/FTF has been well documented in reference 9. As described, the flow over the FTF is perceived as quasi-two-dimensional. As part of the present experiment, preliminary flight tests were completed to verify the assumption of quasi-two-dimensional flow. These flights acquired baseline data for the smooth-panel configuration. These and all subsequent flights were flown with transition strips located, as shown in figure 3, on both sides of the FTF to ensure turbulent flow.

The chordwise and spanwise pressure distributions were closely monitored during the smooth flights to assess the quality of the flow environment. There were two main concerns: (1) whether there were any Mach number effects on the pressure distributions that might influence the riblet performance and its interpretation; and (2) whether the variations in pressure distribution from one flight condition to another would adversely affect the measured flow properties.

Figure 7 shows the development of chordwise pressure distribution as a function of Mach number for Mach 1.2 to 1.6. The chordwise pressure distributions show a region of strong pressure gradient associated with the shock across the FTF, as indicated by the sharp rise in pressure apparent in these figures. As expected, figures 7(a) to (e) illustrate the shock moving aft across the test surface approaching the boundary-layer-rake station at Mach 1.6. The effect of the nearby shock on the velocity profile at Mach 1.6 can be seen in figure 8 as compared with the normal velocity profile at Mach 1.2.

Figure 9 shows representative spanwise pressure distributions measured by the Preston tubes at the trailing edges of the FTF for Mach 1.2 and 1.4. The overall spanwise pressure distributions show minimal pressure gradients along the span of FTF. Measurements from the fourth probe, $z/b = 0.24$, were not included since this probe was located in the wake of the boundary-layer rake.

The effects that variations in chordwise pressure distribution have on the measured flow properties at the aft location of the test surface were further investigated. In flows where the chordwise growth of the boundary layer is fairly slow, the inner portion closest to the wall of a turbulent boundary layer can adjust to the changes in outer flow conditions, in particular pressure gradients. The boundary-layer profile is considered in equilibrium if no time-lag effects are evident (ref. 17). If the pressure gradient is too large, however, the inner portion of the boundary layer cannot adjust fast enough, and the common relationships among skin friction, Reynolds number based on momentum thickness, and shape parameter are no longer valid.

The measured boundary-layer profiles were examined to ascertain equilibrium conditions for the flow. In addition, the profiles were evaluated for three-dimensional characteristics and possible shock interactions that may jeopardize the quality of the data at the measurement station or anywhere else along the riblet surface. Traditionally, two parameter velocity profile families have been found to describe turbulent equilibrium profiles. This means that if two of the three parameters c_f, Re_θ, and H are known, then the third one is uniquely defined (ref. 17). In the present case, since only the computed boundary layer was required to agree in Re_θ (i.e., C_P and θ), deviations in c_f and H between the computations and the experiment were used as an indication of nonequilibrium conditions in the experimental data. Figure 10 compares experimental and computed shape parameters for smooth data. The comparison shows agreement; however, deviations indicate nonequilibrium conditions at Mach 1.6. Note, as shown earlier, that at Mach number of 1.6, a shock occurs at the boundary-layer rake station.

To assess the flow for effects of three dimensionality and shock interaction, the actual velocity profiles in nondimensional wall parameters were examined and compared. Flow behavior at the wall in a turbulent boundary layer is generally expressed in wall scales of length and velocity, $y+$ and $u+$

$$u+ = \frac{u}{u_\tau} \text{ and } y+ = \frac{y u_\tau}{\nu_W}$$

where $u_\tau = \sqrt{\frac{\tau_W}{\rho}}$

Figure 11 shows law-of-the-wall plots for smooth wall data for Mach numbers ranging from 1.2 to 1.41. For the supersonic cases, there was good agreement between the law of the wall and the velocity profiles when plotted in the incompressible form. To account for compressibility effects, it was necessary to transform the profiles to incompressible form. This transformation was computed using the compressibility parameter proposed by Gaudet (ref. 7)

$$u_{\tau \text{ inc}} = u_{\tau}\sqrt{F_c}$$

where $F_c = 1 = \frac{2M_e^2}{20+M_e}$

The estimated values for skin friction are clearly in good agreement with the physical characteristics, and the profiles are in equilibrium at this location. An error in c_f would have created a shift of the line, and nonequilibrium characteristics would have caused an error in level and slope. Since the values obtained for the skin friction are acceptable, they are concluded also reliable for determining the proper $h+$ values for the riblet surfaces.

Flow angularity effects were also considered. The flow angle is defined as the angle between the longitudinal grooves of the riblet surface and the oncoming flow (fig. 1). Reference 2 reported flow angularity effects to be significant at flow angles greater than 15°. Since the riblet surface is mounted longitudinally on the FTF, changes in aircraft angle of attack corresponded to changes in flow angle as seen by the riblet surface. Trim angle of attack for the aircraft ranged from approximately 0.5° to 5° for all the test cases flown. Since these flow angles were much smaller than 15°, flow angularity effects in this experiment were concluded to be minimal.

Smooth and riblet surface boundary-layer profiles were compared to evaluate the effect of riblets in reducing skin-friction drag. Figure 12 shows typical boundary-layer profiles for smooth and riblet surfaces. Comparison of these boundary-layer profiles indicated a slightly less full boundary-layer profile for the riblet surface, which implied a change in value of momentum thickness. From the differences in momentum thickness between smooth and riblet surfaces, average skin-friction reductions were computed for the 0.0030- and 0.0013-in. riblets.

Figure 13 shows average skin-friction coefficients plotted against unit Reynolds numbers for the smooth and riblet surface test cases for the 0.0030-in. riblets. As expected, average skin friction decreased with Reynolds number and Mach number accordingly. As this figure shows, average skin friction for the riblet surface was consistently less than that for the smooth surface for each Mach number. To make comparisons between the smooth and riblet surface data at exact Reynolds numbers, curve fits through the data were used. The solid lines in these figures represent the curve fits through the data for smooth and riblet surfaces, accordingly. These curves should only be interpreted to be accurate within the range of data.

Figure 14 shows average skin-friction reduction plotted against unit Reynolds number for the 0.0030-in. riblets. These skin-friction reductions ranged from 4 to 8 percent for Mach 1.2 to 1.6 and Reynolds numbers from 2 to 3.4 million Re/ft. These figures also show the design Reynolds number range. As can be noted from the figure, however, maximum skin-friction reduction occurred at larger

Reynolds numbers than expected in all cases for the 0.0030-in. riblets. A 4- to 5.5-percent average skin-friction reduction resulted within the design Reynolds number range and a 4.5- to 8-percent reduction resulted outside this range. For the cases shown, skin-friction reductions increased with Reynolds number but showed little effect for increasing Mach number.

Figure 15 shows average skin-friction coefficients plotted against unit Reynolds number for the smooth surface and the surface with 0.0013-in. riblets. These results showed skin-friction coefficients for the riblet surface to be generally less than the corresponding values for smooth surfaces as seen for the 0.0030-in. riblets. As in the previous figure, average skin friction decreased with Reynolds number and Mach number accordingly.

Figure 16 shows average skin-friction reductions for the 0.0013-in. riblets plotted against unit Reynolds number. These results ranged from 4 to 15 percent for Mach 1.2 to 1.4 and Reynolds numbers ranging from 3.6 to 6 million Re/ft. In addition, skin-friction reductions increased with Reynolds number and, similar to the results for the 0.0030-in. riblets, showed little effect for increasing Mach number.

Figures 14 and 16 show the design Reynolds number ranges. These results show skin-friction reductions beyond the upper and below the lower limits of the Reynolds number range. Maximum skin-friction reduction for the 0.0013-in. riblets occurred beyond the upper Reynolds number range at Mach 1.2 and below the lower Reynolds number range at Mach 1.4. Although a general reduction in skin friction is apparent, trends are difficult to substantiate because of the scatter and limited data.

Figure 17 shows percentage difference of drag coefficient compared with nondimensional riblet height, $h+$, adjusted for incompressible conditions for the 0.0030-in. riblets as an example. As seen from this figure, the $h+$ values ranged from 9 to 15 in general. This result was in good agreement with results of previous subsonic flow investigations (refs. 1 and 2), which found $h+$ values of 12 to 15 to yield maximum skin-friction drag reduction.

CONCLUDING REMARKS

A flight experiment was conducted on the flight test fixture of an F-104G aircraft to test the skin-friction drag reduction characteristics of riblets at supersonic speeds. Average skin-friction results were determined from boundary-layer profiles for smooth and riblet surfaces. Test points were selected from a design and off-design Reynolds number range based on subsonic wind-tunnel data.

Flight test results for the 0.0030-in. riblets showed skin-friction reductions of 4 to 8 percent for Mach numbers ranging from 1.2 to 1.6 and Reynolds numbers ranging from 2 to 3.4 million Re/ft. The results for the 0.0013-in. riblets also showed skin-friction reductions that ranged from 4 to 15 percent for Mach 1.2 to 1.4 and Reynolds numbers of 3.6 to 6 million Re/ft. The effectiveness of both riblet sizes increased with Reynolds number, even above the design Reynolds number range, and showed little variation with Mach number.

The nondimensional riblet height values, $h+$, ranged from 9 to 15 in general. This result was in good agreement with results of previous subsonic flow investigations, which found $h+$ values of 12 to 15 to yield maximum skin-friction drag reduction.

REFERENCES

1. Walsh, Michael J., "Riblets," *in Viscous Drag Reduction in Boundary Layers*, American Institute of Aeronautics and Astronautics, Inc., Washington, DC, 1990, p. 203–261.

2. Walsh, M.J. and A.M. Lindemann, "Optimization and Application of Riblets for Turbulent Drag Reduction," AIAA Paper 84-0347, 22d Aerospace Sciences Meeting, Reno, NV, Jan. 9–12, 1984.

3. Walsh, M.J., W.L. Sellers, III, and C.B. McGinley, "Riblet Drag Reduction at Flight Conditions," AIAA-88-2554, June 1988.

4. Reidy, Laurel W. and Greg W. Anderson, "Drag Reduction for External and Internal Boundary Layers Using Riblets and Polymers," AIAA-88-0138, Jan. 1988.

5. McLean, J. Douglas, Dezso N. George-Falvy, and Peter P. Sullivan, "Flight-Test of Turbulent Skin-Friction Reduction by Riblets," *in Turbulent Drag Reduction by Passive Means*, presented at the Turbulent Drag Reduction by Passive Means Conference, London, England, Sept. 15–17, 1987, p. 408–424.

6. Coustols, E., J. Cousteix, and J. Belanger, "Drag Reduction Performance on Riblet Surfaces and Through Outer Layer Manipulators," *in Turbulent Drag Reduction by Passive Means*, presented at the Turbulent Drag Reduction by Passive Means Conference, London, England, Sept. 15–17, 1987, p. 250–289.

7. Gaudet, L., "Properties of Riblets at Supersonic Speed," *Applied Scientific Research*, vol. 46, pp. 245–254, 1989.

8. Robinson, Stephen K., "Effects of Riblets on Turbulence in a Supersonic Boundary Layer," AIAA-88-2526, June 1988.

9. Meyer, Robert R., Jr., *A Unique Flight Test Facility: Description and Results*, NASA TM-84900, 1982.

10. Petersohn, Erik, *Concerning an Investigation of the Flow in Pipes, Internally Covered with Shark Skin*, AE-I-444, FFA, The Aeronautical Research Institute of Sweden, 1959.

11. Choi, Kwing-So, "Near-Wall Structure of a Turbulent Boundary Layer with Riblets," *J. Fluid Mech.*, vol. 208, Nov. 1989, pp. 417–458.

12. Meyer, Robert R., Jr. and Edward T. Schneider, "Real-Time Pilot Guidance for Improved Flight Test Maneuvers," AIAA-83-2747, Nov. 1983.

13. Braslow, Albert L. and Eugene C. Knox, *Simplified Method for Determination of Critical Height of Distributed Roughness Particles for Boundary-Layer Transition at Mach Numbers from 0 to 5*, NACA TN-4363, 1958.

14. Bertelrud, Arild, "Preston Tube Calibration Accuracy," *AIAA Journal*, vol. 14, no. 1, Jan. 1976, pp. 98–100.

15. Richardson, Norman R. and Albin O. Pearson, *Wind-Tunnel Calibrations of a Combined Pitot-Static Tube, Vane-Type Flow-Direction Transmitter, and Stagnation-Temperature Element at Mach Numbers from 0.60 to 2.87*, NASA TN-D-122, 1959.

16. Bradshaw, P., K. Unsworth, and G.A. Mizner, *Calculation of Compressible Turbulent Boundary Layers with Heat Transfer on Straight-Tapered Swept Wing*, *AIAA Journal*, vol. 14, Mar. 1976, p. 399–400.

17. Schlichting, H., *Boundary-Layer Theory*, McGraw-Hill Book Co., New York, NY, 1968.

18. Squire, H.B. and A.D. Young, *The Calculation of the Profile Drag of Aerofoils*, ARC R & M 1838, 1937.

19. Lock, R.C., "Prediction of the Drag of Wings at Subsonic Speeds by Viscous/Inviscid Interaction Techniques," AGARD Report 723, *Aircraft Drag Prediction and Reduction*, 1985.

Table 1. Boundary-layer-rake probe heights.

Rake probe no.	Distance of rake probe above surface, in.
1	0.025
2	0.040
3	0.095
4	0.150
5	0.190
6	0.250
7	0.290
8	0.350
9	0.400
10	0.500
11	0.650
12	0.850
13	1.000
14	1.250
15	1.450
16	1.650
17	1.900
18	2.100
19	2.300
20	2.500

Table 2. Static pressure orifice locations for upper and lower stations on flight test fixture.

Pressure tap no.	Horizontal distance from leading edge, in.	x/c
1	3.24	0.04
2	6.48	0.08
3	9.72	0.12
4	13.06	0.16
5	21.00	0.26
6	27.00	0.33
7	33.00	0.41
8	39.00	0.48
9	45.00	0.55
10	51.00	0.63
11	57.00	0.70
12	63.00	0.77
13	69.00	0.85
14	75.00	0.93

Table 3. Preston tube measurement locations.

Preston tube no.	Distance from bottom of flight test fixture to Preston tube, in.	z/b
1	17.50	0.730
2	15.55	0.650
3	13.55	0.560
4*	5.85	0.240
5	3.85	0.160
6	1.80	0.075

* Note: Measurements from this probe not used in the data analysis.

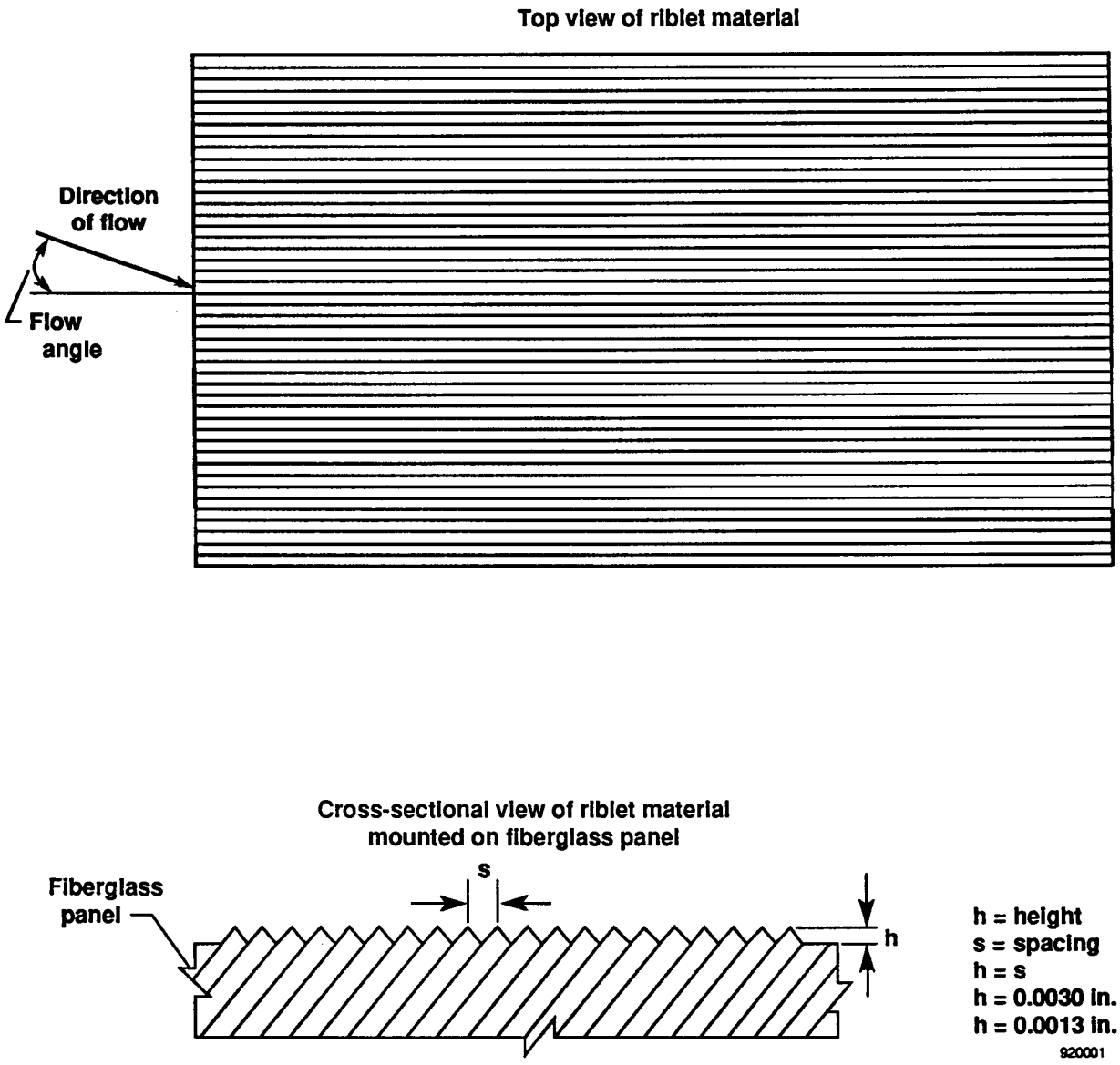

Figure 1. Riblet material.

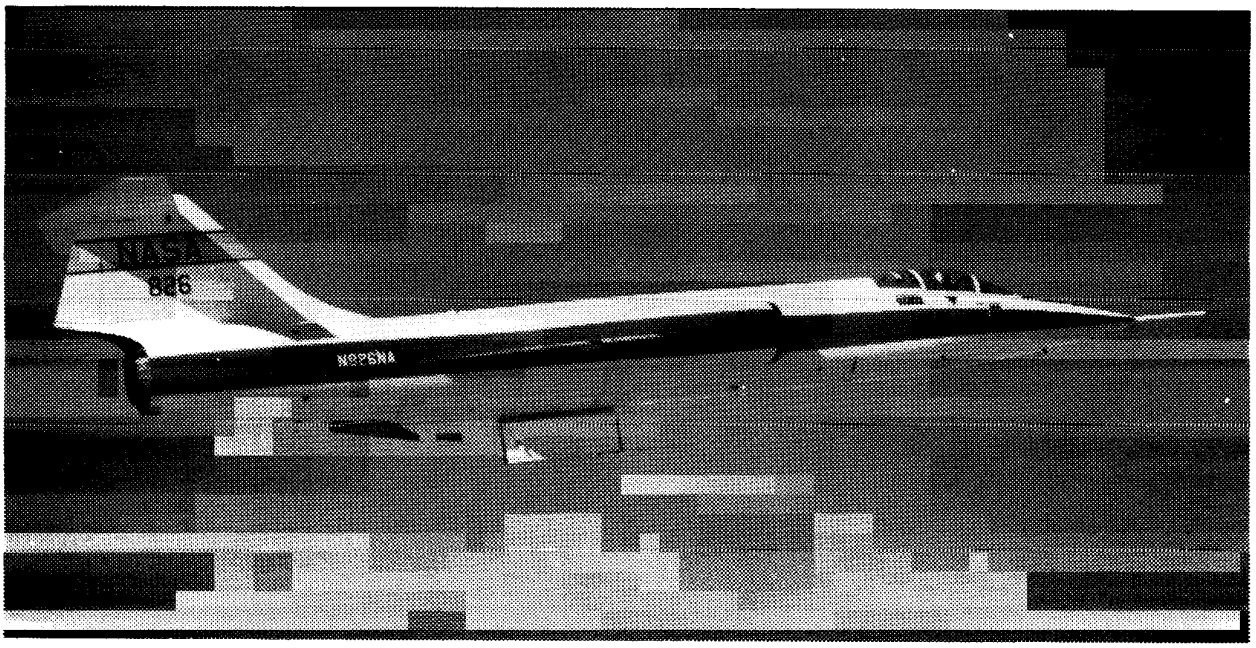

EC89 0011-4

(a) Mounted on F-104G aircraft.

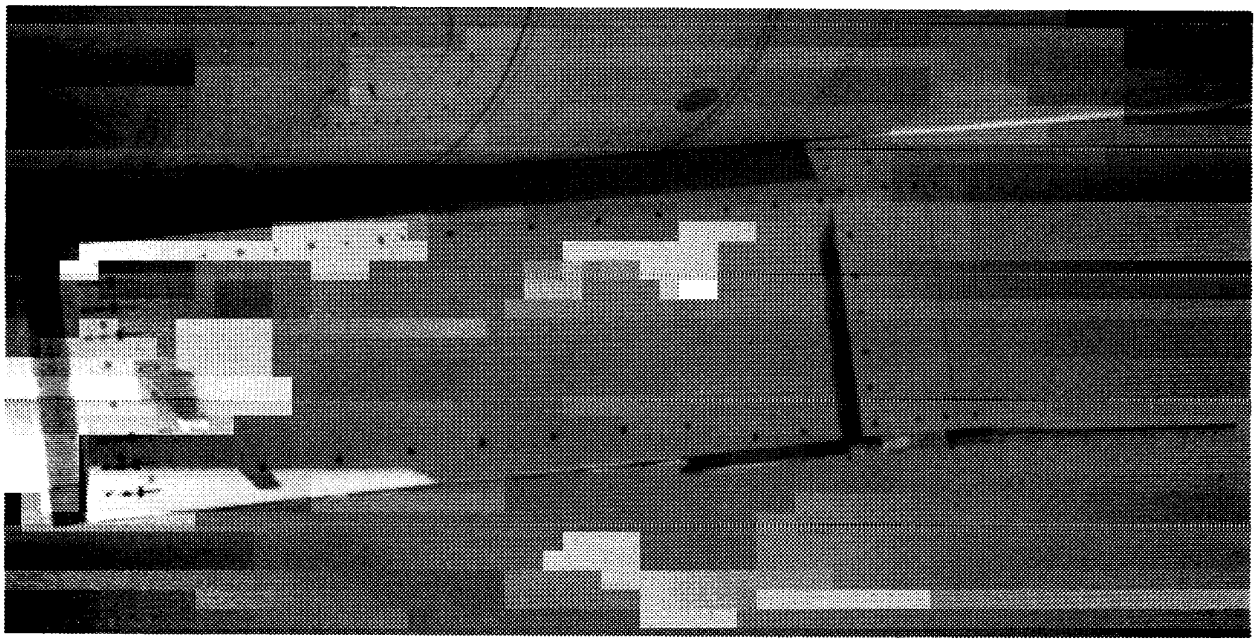

EC89 0011-8

(b) Close up view.

Figure 2. Flight test fixture.

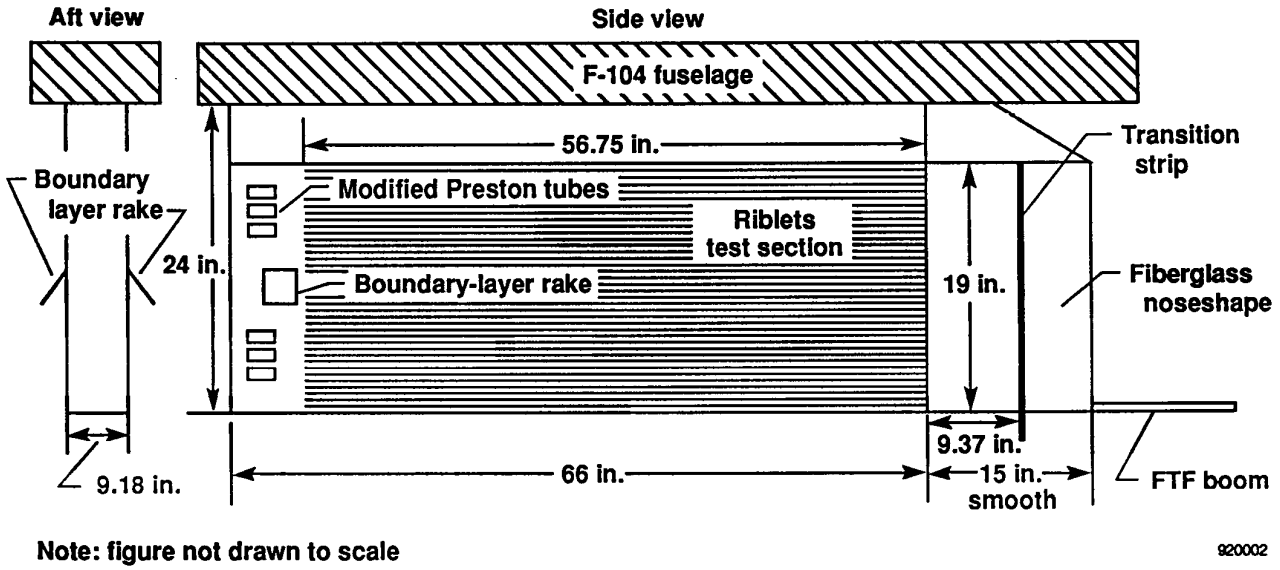

(a) Right side.

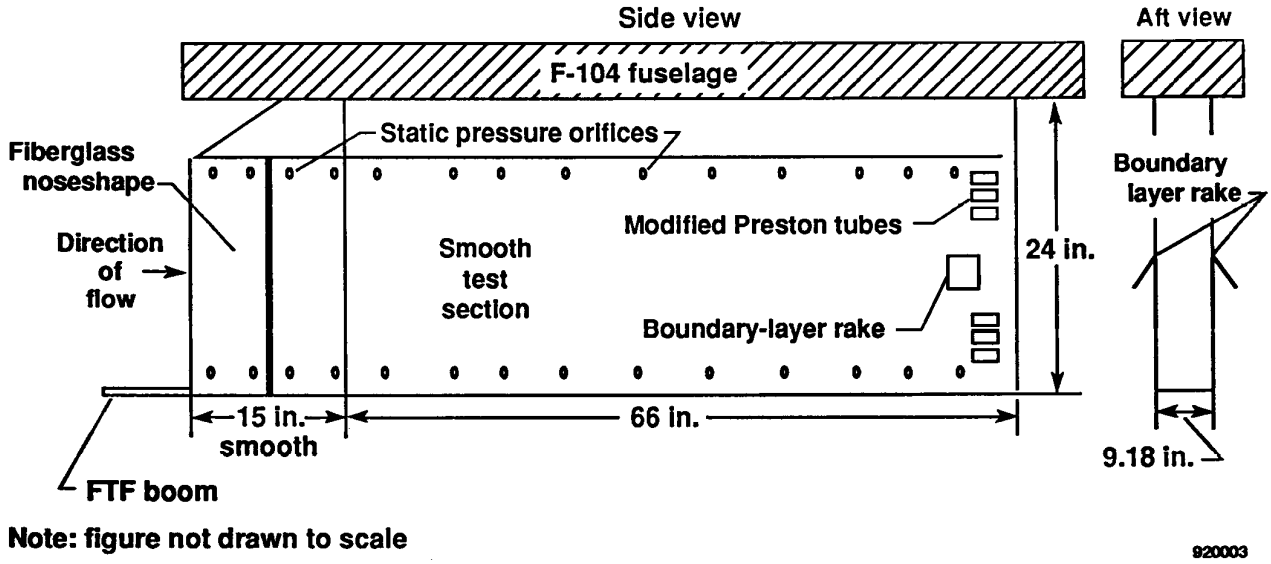

(b) Left side.

Figure 3. Flight test fixture experiment setup.

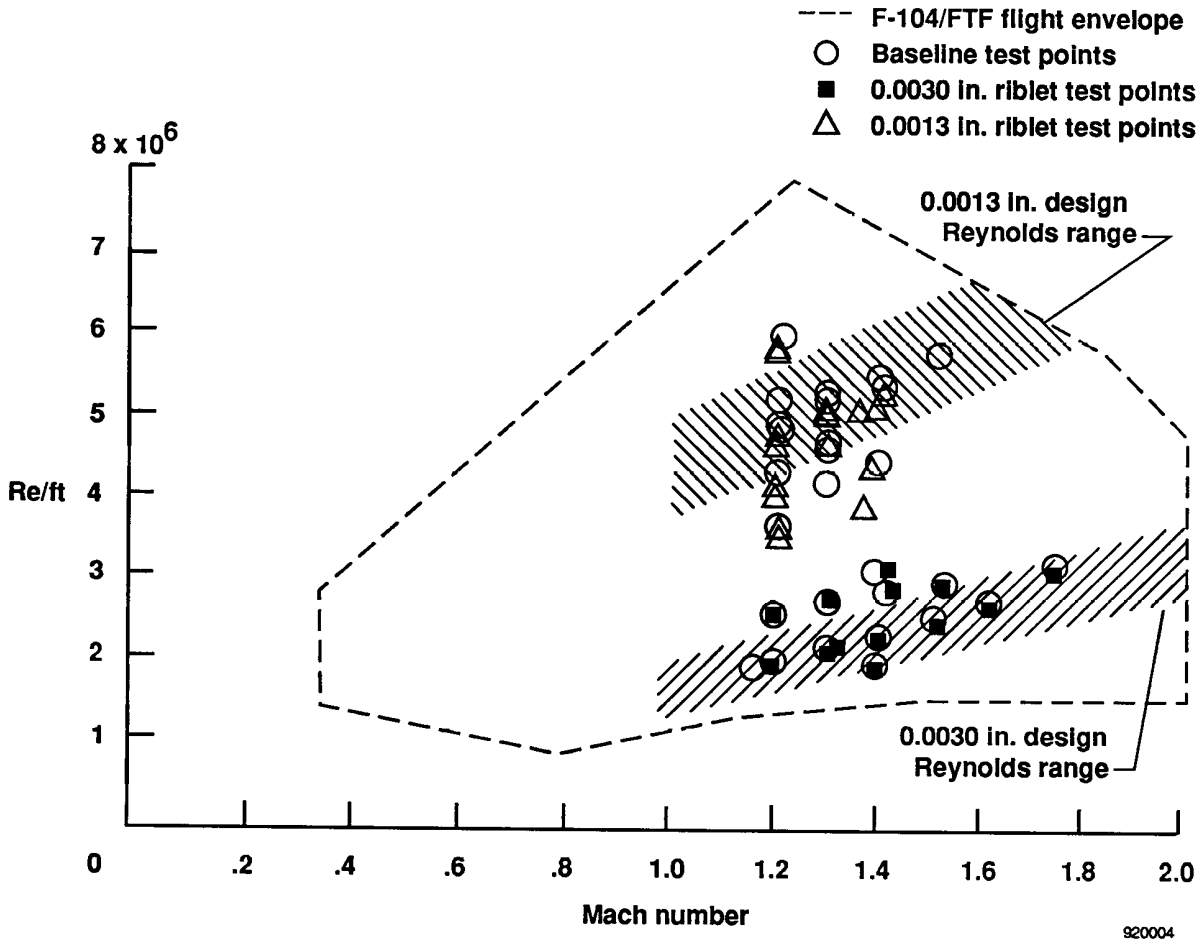

Figure 4. Flight envelope for F-104G including flight test points.

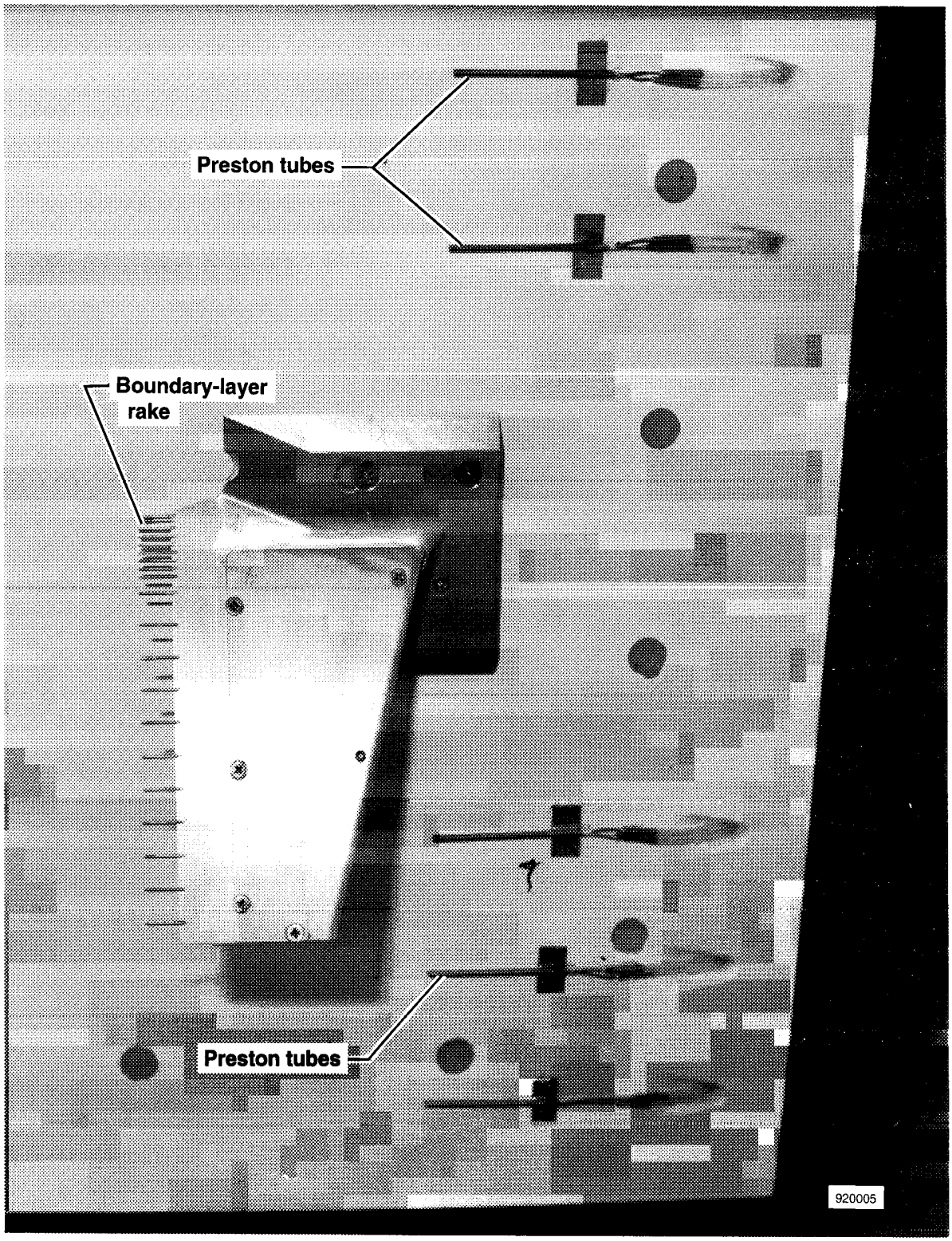

Figure 5. Boundary-layer rake and Preston tubes mounted on flight test fixture.

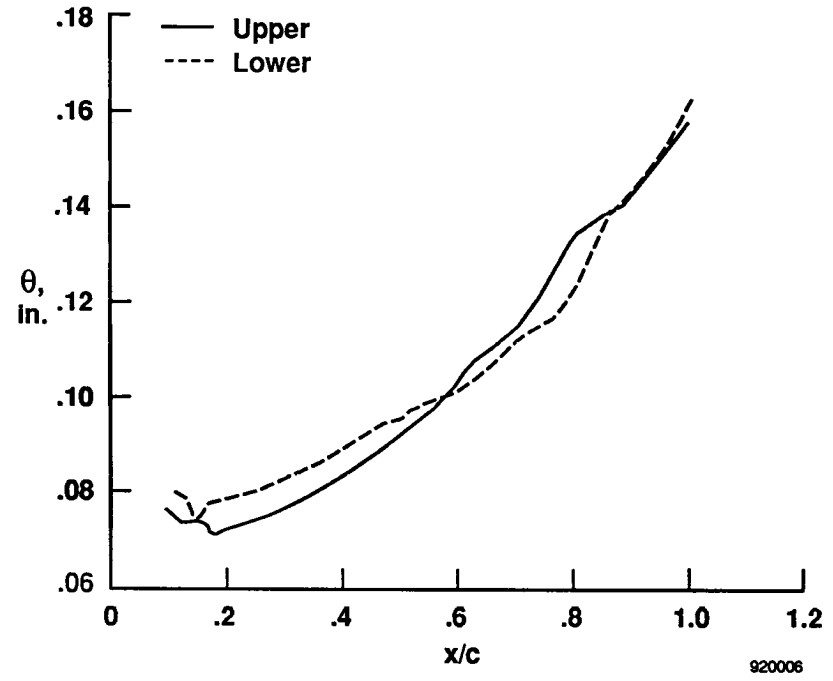

(a) Momentum thickness distribution.

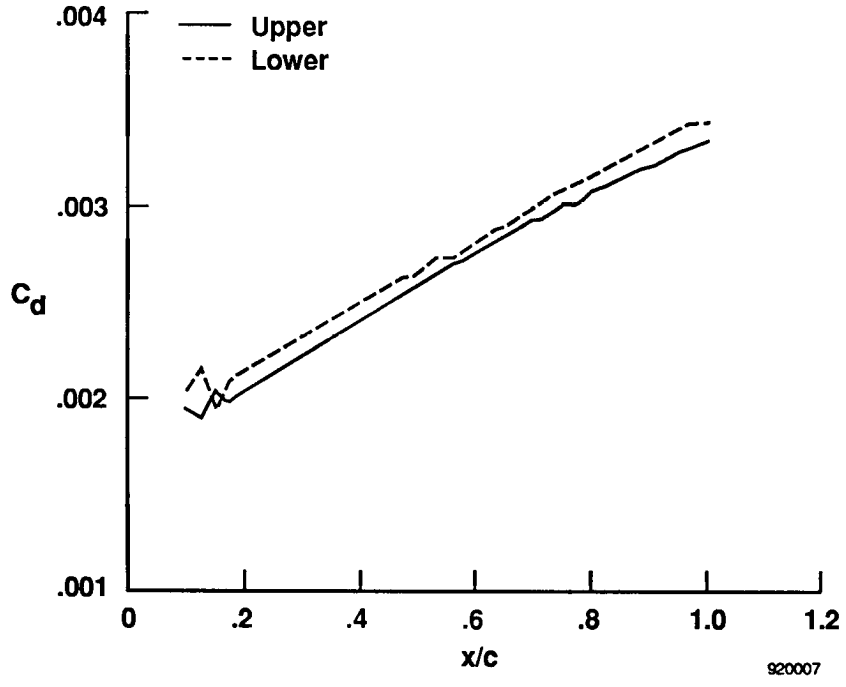

(b) Local drag coefficient distribution.

Figure 6. Estimated distributions for upper and lower pressure orifice rows of the flight test fixture at Mach 1.6.

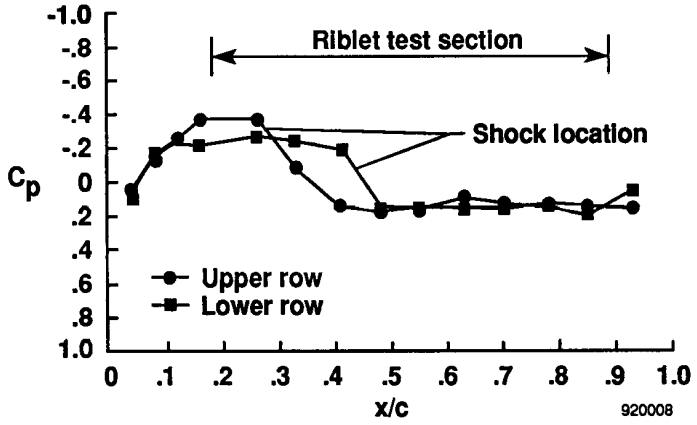

(a) Mach 1.2.

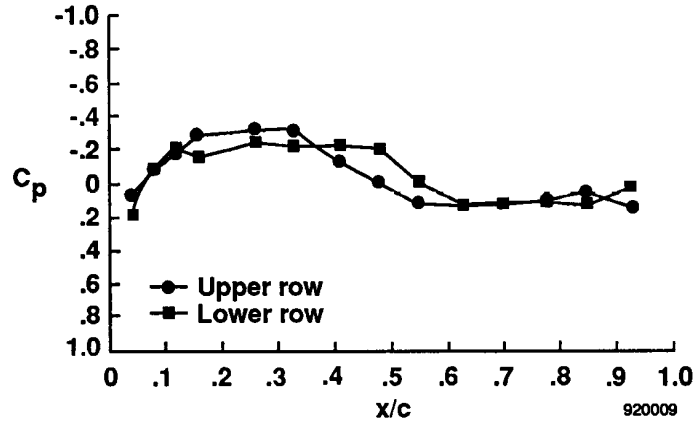

(b) Mach 1.3.

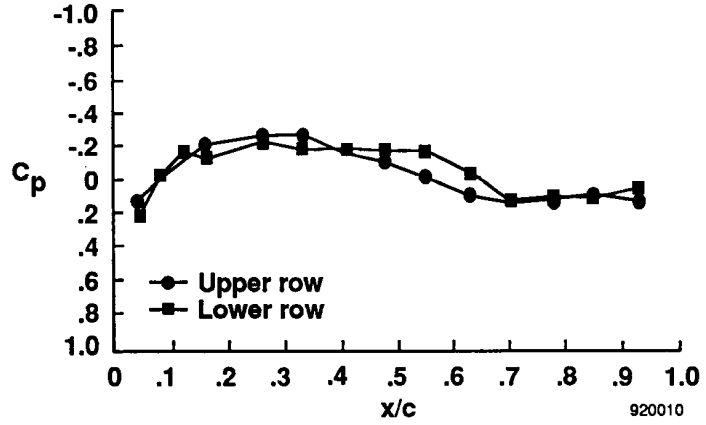

(c) Mach 1.4.

Figure 7. Chordwise pressure distributions for flight test fixture at specified Mach numbers.

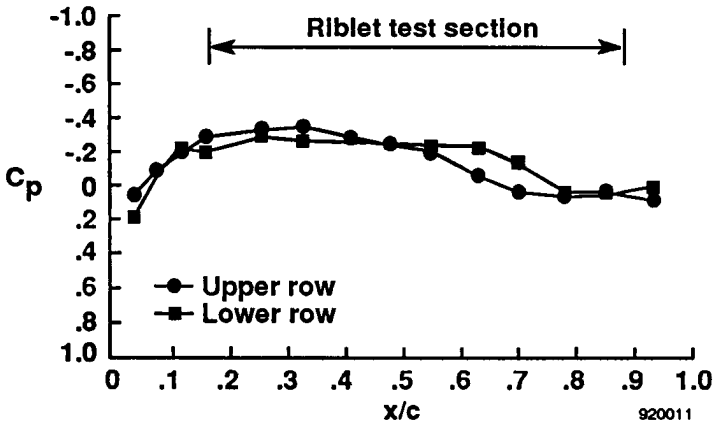

(d) Mach 1.5.

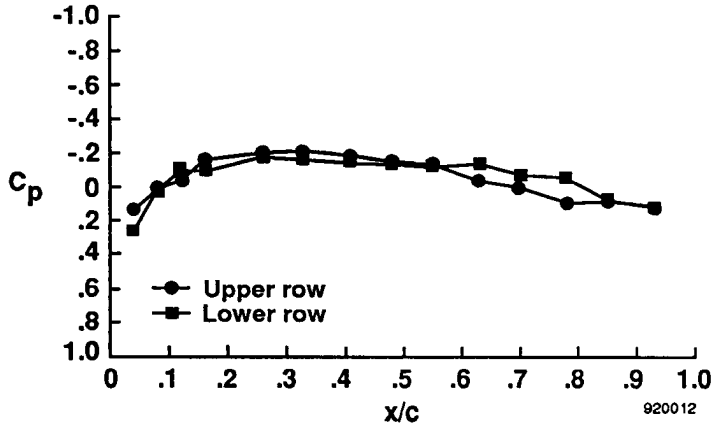

(e) Mach 1.6.

Figure 7. Concluded.

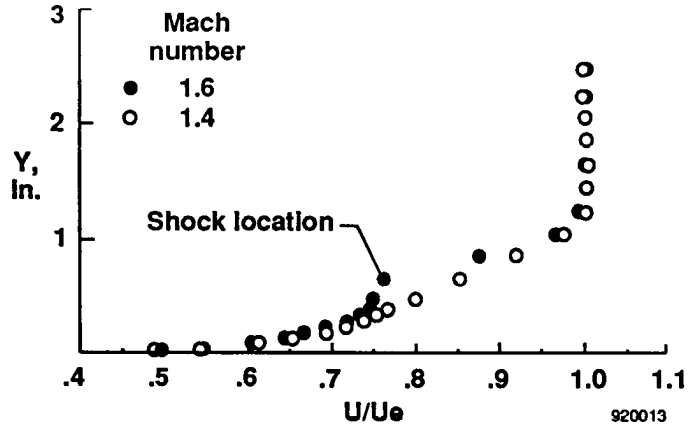

Figure 8. Boundary-layer profiles at Mach 1.6 and 1.4.

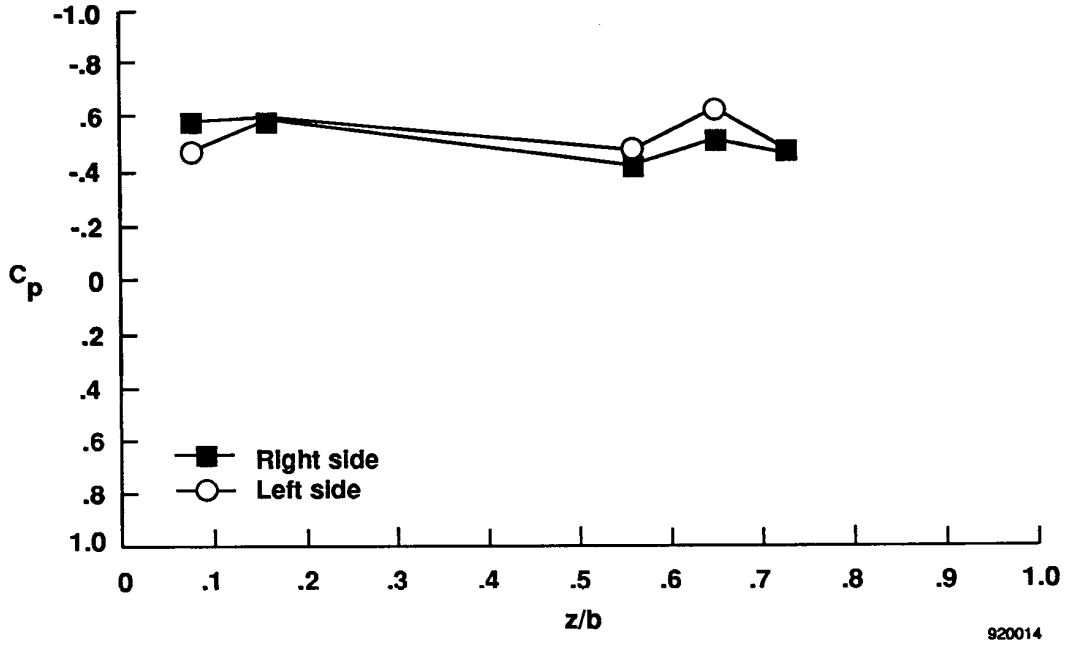

(a) Mach 1.2.

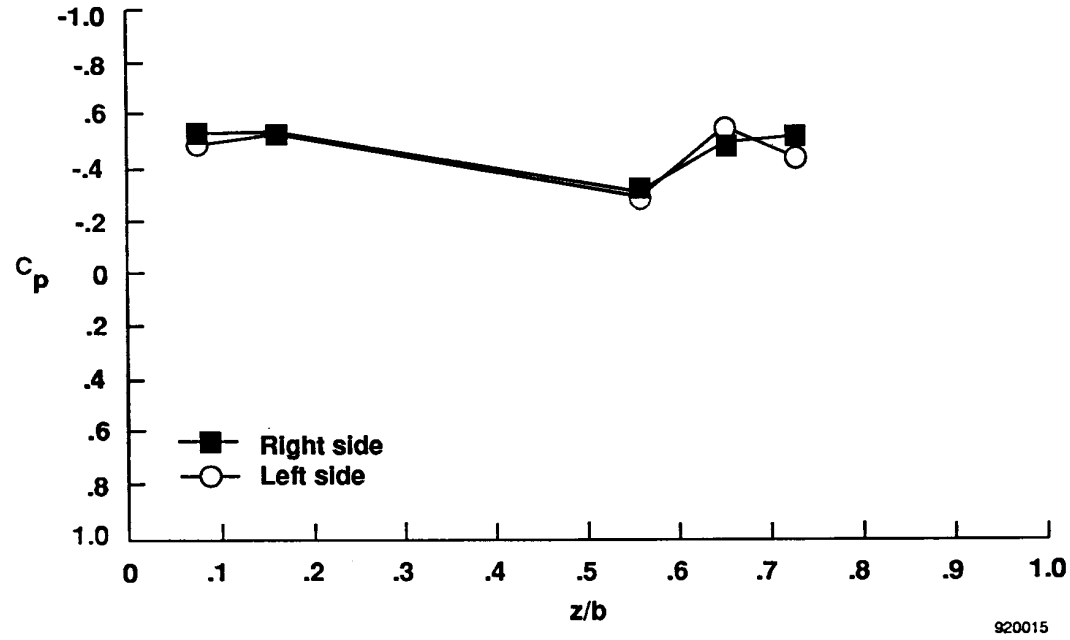

(b) Mach 1.4.

Figure 9. Spanwise pressure distributions for flight test fixture for chord location $x/c = 0.93$ at specified Mach numbers.

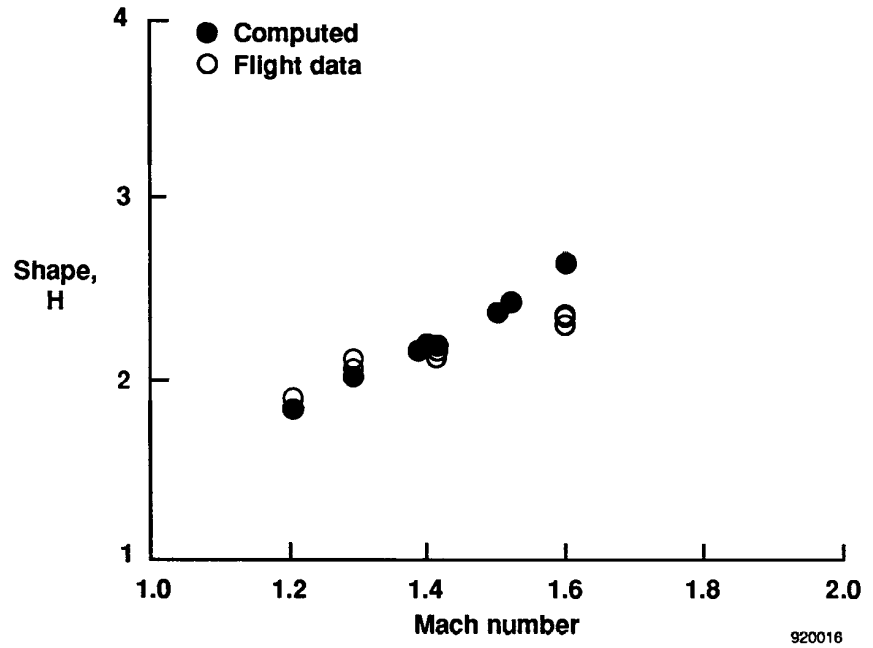

Figure 10. Comparison of shape parameter for computed and flight-measured results.

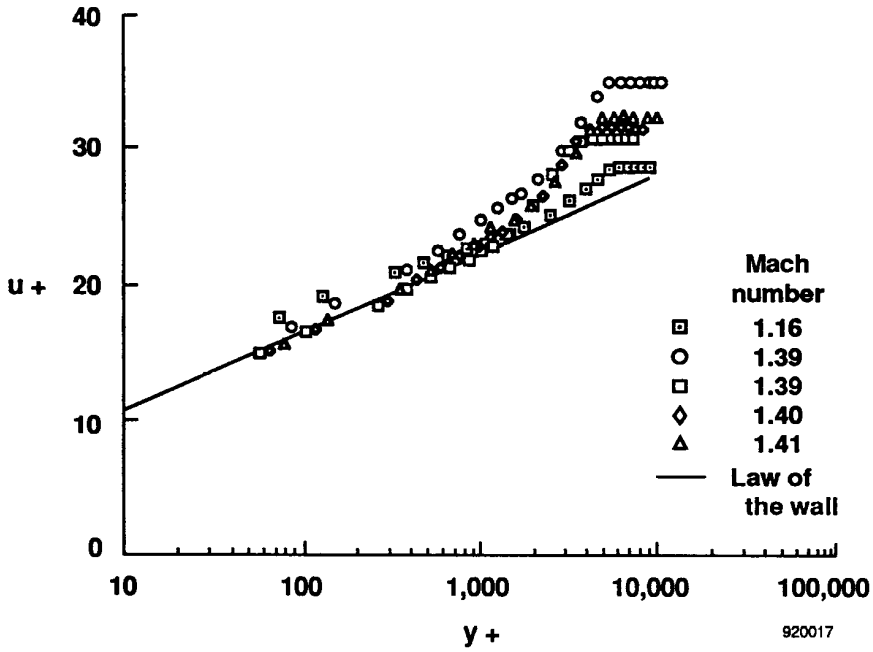

Figure 11. Transformed flight-velocity profiles in wall coordinates incompressible form.

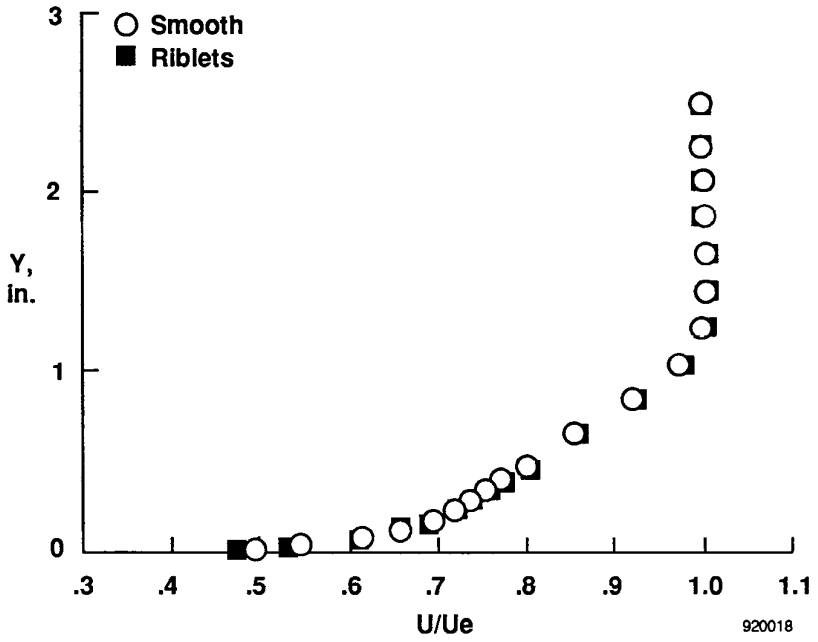

(a) Mach 1.4 and Re/ft 2.95E6 for 0.0030-in. riblets.

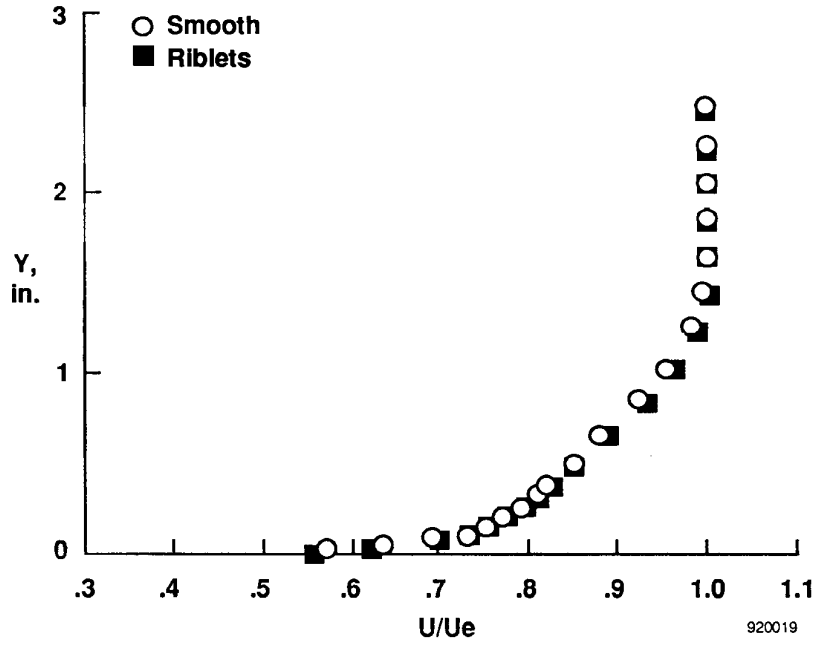

(b) Mach 1.2 and Re/ft 4.85E6 for 0.0013-in. riblets.

Figure 12. Typical boundary-layer profiles for smooth and riblet surfaces.

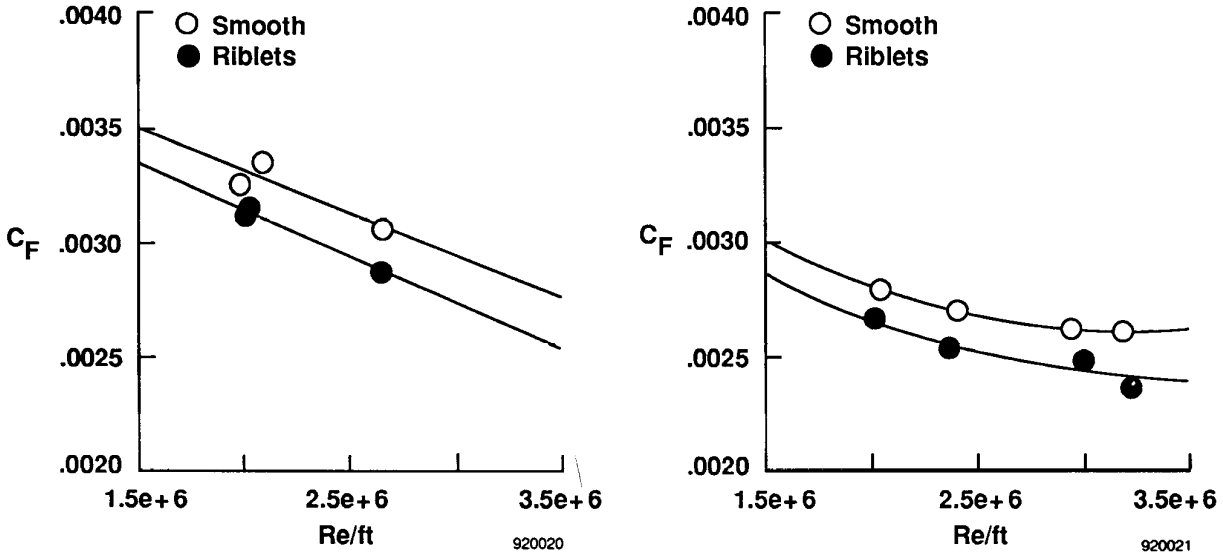

(a) Mach 1.2.

(b) Mach 1.4.

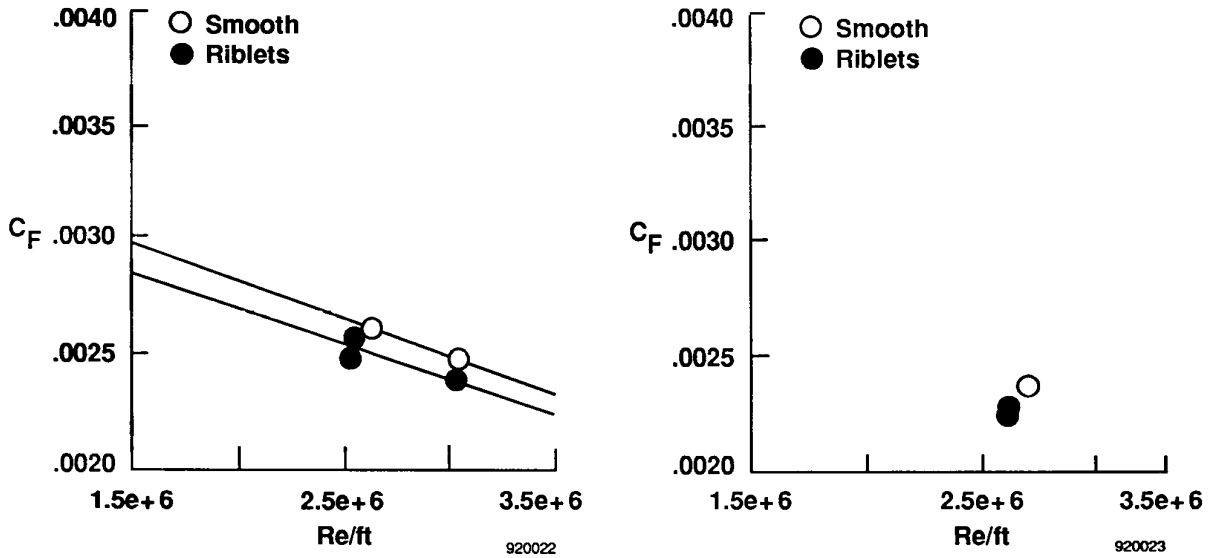

(c) Mach 1.5.

(d) Mach 1.6.

Figure 13. Average skin-friction coefficients for 0.0030-in. riblets compared with unit Reynolds number for Mach 1.2 to 1.6.

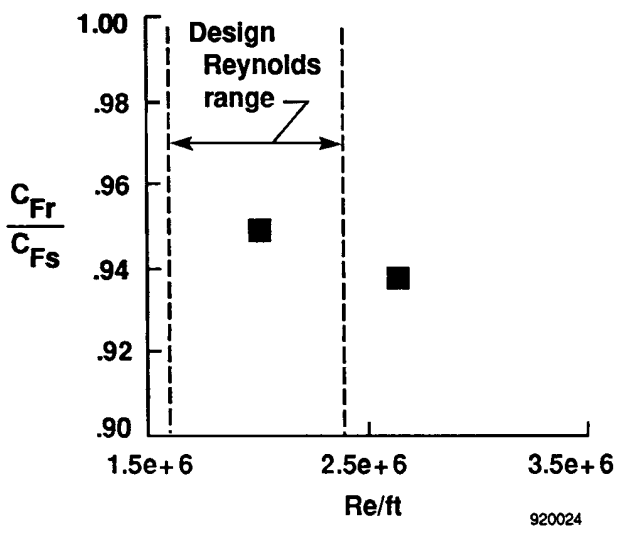

(a) Mach 1.2.

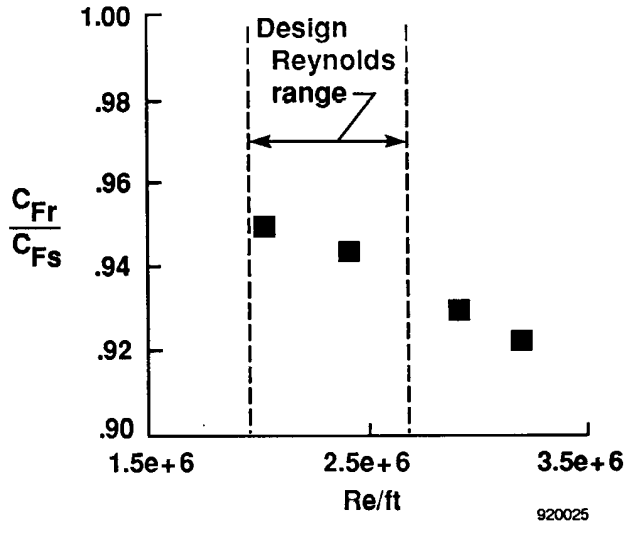

(b) Mach 1.4.

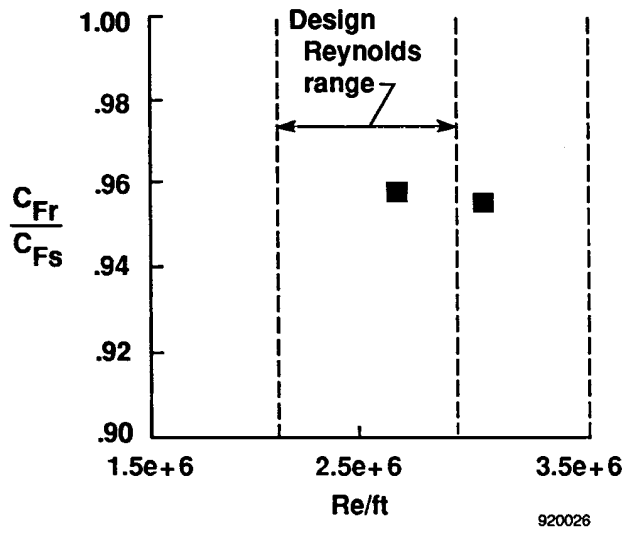

(c) Mach 1.5.

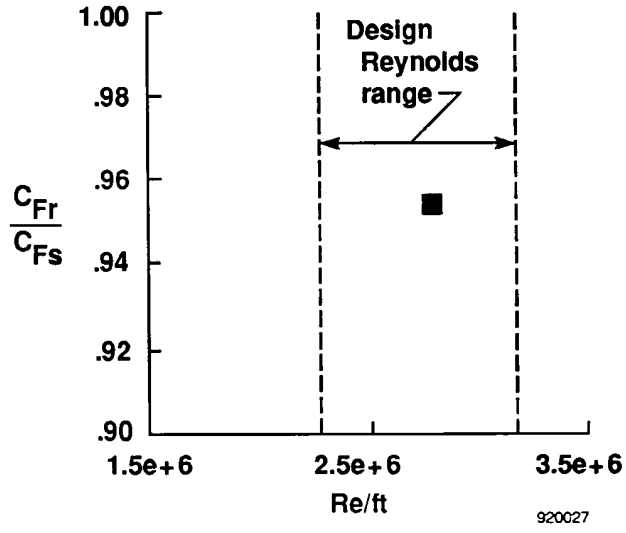

(d) Mach 1.6.

Figure 14. Average skin-friction reduction for 0.0030-in. riblets compared with unit Reynolds number for Mach 1.2 to 1.6.

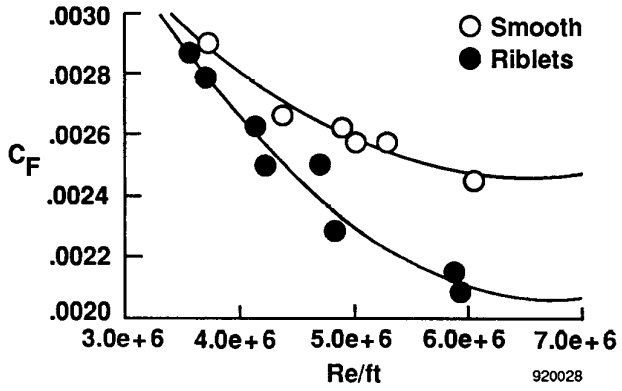

(a) Mach 1.2.

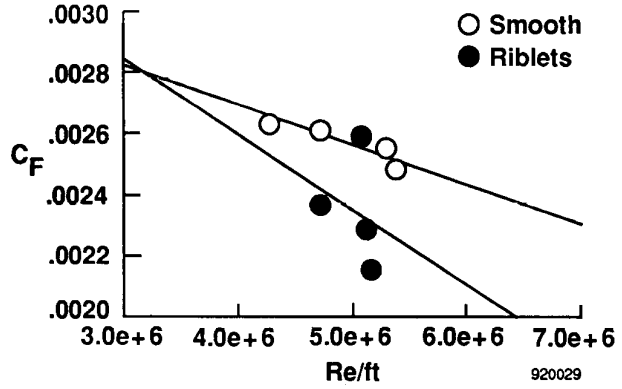

(b) Mach 1.3.

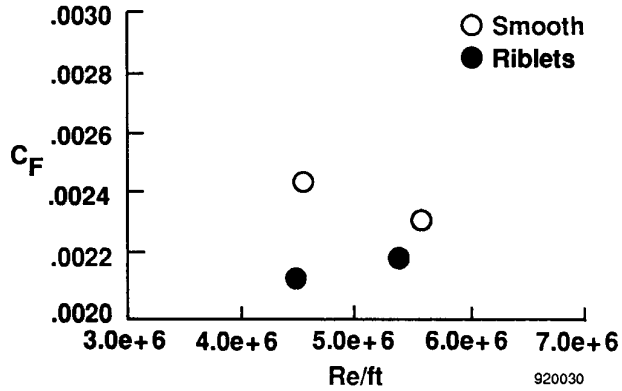

(c) Mach 1.4.

Figure 15. Average skin-friction coefficient for 0.0013-in. riblets compared with unit Reynolds number for Mach 1.2 to 1.4.

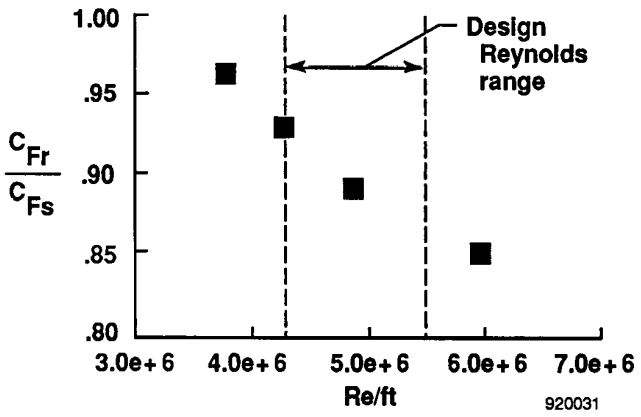

(a) Mach 1.2.

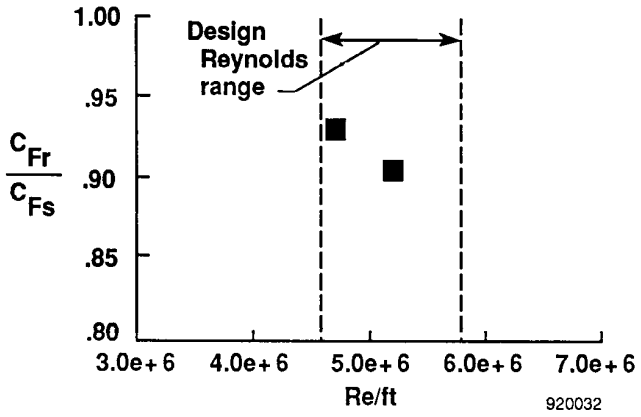

(b) Mach 1.3.

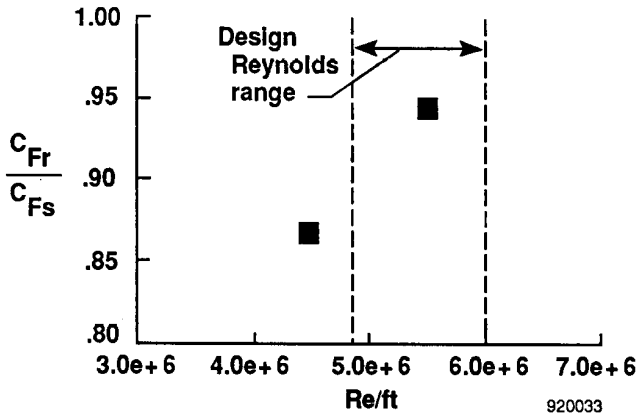

(c) Mach 1.4.

Figure 16. Average skin-friction reduction for 0.0013-in. riblets compared with unit Reynolds number for Mach 1.2 to 1.4.

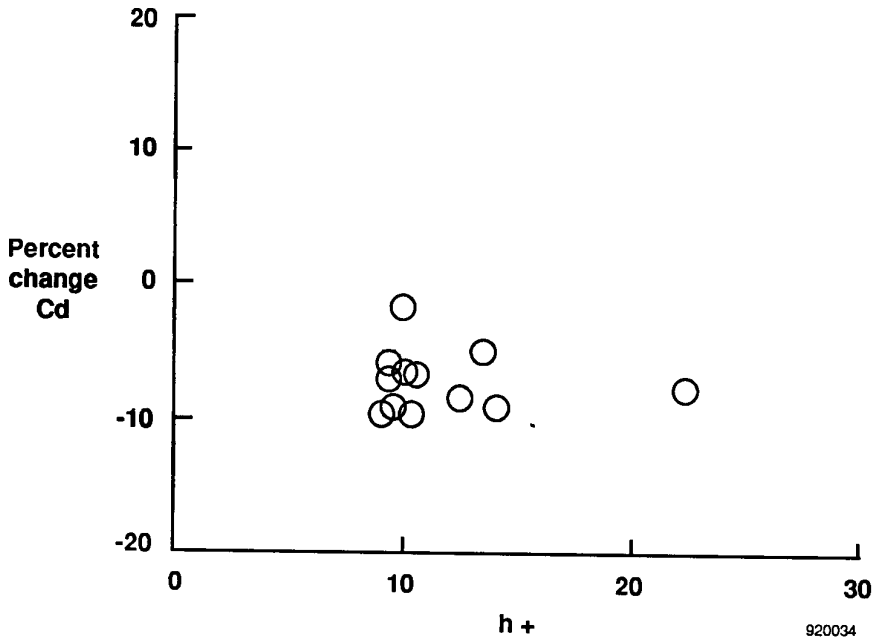

Figure 17. Percentage difference of drag coefficient for 0.0030-in. riblets compared with average riblet height incompressible form.

REPORT DOCUMENTATION PAGE

Form Approved
OMB No. 0704-0188

1. AGENCY USE ONLY *(Leave blank)*	2. REPORT DATE	3. REPORT TYPE AND DATES COVERED
	June 1992	Technical Memorandum

4. TITLE AND SUBTITLE

Flight Test Results of Riblets at Supersonic Speeds

5. FUNDING NUMBERS

WU-505-60-21

6. AUTHOR(S)

Fanny A. Zuniga, Bianca T. Anderson, and Arild Bertelrud

7. PERFORMING ORGANIZATION NAME(S) AND ADDRESS(ES)

NASA Dryden Flight Research Facility
P.O. Box 273
Edwards, CA 93523-0273

8. PERFORMING ORGANIZATION REPORT NUMBER

H-1774

9. SPONSORING/MONITORING AGENCY NAME(S) AND ADDRESS(ES)

National Aeronautics and Space Administration
Washington, DC 20546-0001

10. SPONSORING/MONITORING AGENCY REPORT NUMBER

NASA TM-4387

11. SUPPLEMENTARY NOTES

Fanny A. Zuniga and Bianca T. Anderson: NASA Dryden Flight Research Facility, Edwards, California
Arild Bertelrud: High Technology Corporation, Hampton, Virginia

12a. DISTRIBUTION/AVAILABILITY STATEMENT

FEDD

Subject Category 02

12b. DISTRIBUTION CODE

13. ABSTRACT ***(Maximum 200 words)***

A flight experiment to test and evaluate the skin-friction drag characteristics of a riblet surface in turbulent flow at supersonic speeds was conducted at NASA Dryden Flight Research Facility. Riblets of groove sizes 0.0030 and 0.0013 in. were mounted on the F-104G flight test fixture. The test surfaces were surveyed with boundary-layer rakes and pressure orifices to examine the boundary-layer profiles and pressure distributions of the flow. Skin-friction reductions caused by the riblet surface were reported based on measured differences of momentum thickness between the smooth and riblet surfaces obtained from the boundary-layer data. Flight-test results for the 0.0030-in. riblets show skin-friction reductions of 4 to 8 percent for Mach numbers ranging from 1.2 to 1.6 and Reynolds numbers ranging from 2 to 3.4 million per unit foot. The results for the 0.0013-in. riblets show skin-friction reductions of 4 to 15 percent for Mach 1.2 to 1.4 and Reynolds numbers ranging from 3.6 to 6 million per unit foot.

14. SUBJECT TERMS	15. NUMBER OF PAGES
Riblets; Skin-friction reduction; Supersonic turbulent boundary layers	37
	16. PRICE CODE

17. SECURITY CLASSIFICATION OF REPORT	18. SECURITY CLASSIFICATION OF THIS PAGE	19. SECURITY CLASSIFICATION OF ABSTRACT	20. LIMITATION OF ABSTRACT
Unclassified	Unclassified		